Mapping the UDP-glucuronic Acid Binding Site in UDP-glucuronosyltransferase-1A10 by Homology-Based Modeling: Confirmation with Biochemical Evidence[†]

Rajat Banerjee, Matthew W. Pennington, Amanda Garza, and Ida S. Owens*

Heritable Disorders Branch, National Institute of Child Health and Human Development, National Institutes of Health, Bethesda, Maryland 20892-1830

Received April 7, 2008; Revised Manuscript Received May 16, 2008

ABSTRACT: The UDP-glucuronosyltransferase (UGT) isozyme system is critical for protecting the body against endogenous and exogenous chemicals by linking glucuronic acid donated by UDP-glucuronic acid to a lipophilic acceptor substrate. UGTs convert metabolites, dietary constituents, and environmental toxicants to highly excretable glucuronides. Because of difficulties associated with purifying endoplasmic reticulum-bound UGTs for structural studies, we carried out homology-based computer modeling to aid analysis. The search found structural homology in *Escherichia coli* UDP-galactose 4-epimerase. Consistent with predicted similarities involving the common UDP moiety in substrate/inhibitor, UDP-glucose and UDP-hexanol amine caused competitive inhibition by Lineweaver−Burk plots. Among predicted binding sites N292, K314, K315, and K404 in UGT1A10, two informative sets of mutants K314R/Q/A/E/G and K404R/E had null activities or 2.7-fold higher/50% less activity, respectively. Scatchard analysis of binding data of the affinity ligand, 5-azidouridine-[β-^{32}P]diphosphoglucuronic acid, to purified UGT1A10-His or UGT1A7-His revealed high- and low-affinity binding sites. 2-Nitro-5-thiocyanobenzoic acid-digested UGT1A10-His bound with the radiolabeled affinity ligand revealed an 11.3 and 14.3 kDa peptide associated with K314 and K404, respectively, in a discontinuous SDS−PAGE system. Similar treatment of 1A10His-K314A bound with the ligand lacked both peptides; 1A10-HisK404R- and 1A10-HisK404E showed 1.3-fold greater and 50% less label in the 14.3 kDa peptide, respectively, compared to 1A10-His without affecting the 11.3 kDa peptide. Scatchard analysis of binding data of the affinity ligand to 1A10His-K404R and -K404E showed a 6-fold reduction and a large increase in K_d, respectively. Our results indicate that K314 and K404 are required UDP-glcA binding sites in 1A10, that K404 controls activity and high-affinity sites, and that K314 and K404 are strictly conserved in 70 aligned UGTs, except for S321, equivalent to K314, in UGT2B15 and 2B17 and I321 in the inactive UGT8, which suggests UGT2B15 and 2B17 contain suboptimal activity. Hence our data strongly support UDP-glcA binding to K314 and K404 in UGT1A10.

UGT isozymes carry out the critical role of detoxifying innumerable structurally diverse chemicals encountered on a regular basis, including toxic metabolites, dietary constituents, environmental carcinogens, and, inadvertently, therapeutic agents. All UGT isozymes, which are distributed primarily in liver, kidney, and gastrointestinal tract, transfer glucuronic acid from the common donor substrate UDP-glucuronic acid (UDP-glcA)[1] to a lipophilic acceptor substrate substituted with a hydroxyl and/or carboxyl group generating excretable glucuronides (*1*). It is established that some 17 UGT isozymes with broad substrate range make up the human chemical defense system (*2*). Whereas bilirubin lethal neurotoxicity is primarily prevented by hepatocyte-distributed UGT1A1 (*3*), the location of this same isozyme in the GI tract mucosa (*2, 4*) allows it to convert and inactivate numerous dietary agents, common environmental mutagens, and carcinogens. To the contrary, there is an immeasurable loss in therapeutic benefit as these same GI-distributed isozymes, collectively, convert many medications immediately upon absorption. Because of UGTs capacity to detoxify a vast number of chemicals, an understanding of the mechanism(s) driving glucuronidation will promote strategies to remove toxicants more efficiently, prevent certain chemically based diseases, and extend the half-life of glucuronidatable medications.

Moreover, the discovery that active UGTs require phosphorylation (*4*), necessarily, increases the complexity of mechanism(s) controlling glucuronidation. Hence, it is imperative that we exploit a number of techniques to understand the

[†] This research was supported by the Intramural Research Program of the Eunice Kennedy Shriver NICHD/NIH.

* To whom correspondence should be addressed. E-mail: owensi@mail.nih.gov. Telephone: 301-496-6091. Facsimile: 301-451-4288.

[1] Abbreviations: CHAPS, 3-[(3-cholamidopropyl)dimethylammonio]-1-propanesulfonate; GI, gastrointestinal; KXXX, lysineXXX; KXXXR/G/A/E/G, KXXXarginine/glycine/alanine/glutamate/glycine; MDM, methyl-α-D-mannose pyranoside; NTCB, 2-nitro-5-thiocyanobenzoic acid; NXXX, asparagineXXX; PDB, Protein Data Bank; SXXX, serineXXX; UDP-galactose 4-epimerase, uridine diphosphogalactose 4-epimerase; UDP-glc, UDP-glucose; UDP-glcA, UDP-glucuronic acid; UGT, uridine 5′-diphosphoglucuronosyltransferase; UGT1AX-His, UGT1AX-histidine; 1XEL, UDP-galactose 4-epimerase; YXXX, tyrosineXXX.

10.1021/bi8006127 CCC: $40.75
Published on Web 06/21/2008

process. As UGTs are endoplasmic reticulum bound and are, thus, difficult to purify for crystallization, structural analysis of these isozymes has been difficult. Whereas binding site(s) for the common donor substrate, UDP-glcA, have not been established, this study successfully used homology-based modeling to search the PDB of structurally solved proteins and identified *Escherichia coli* UDP-galactose 4-epimerase (*6, 7*) as having a structural match to a domain in UGT1A10, which includes N292, K314, K315, and K404 predicted to bind UDP-glcA. Biochemical studies confirmed K314 and K404 bind UDP-glcA.

MATERIALS AND METHODS

Homology Modeling of a Human UGT1A10. Homology-based computer modeling was carried out as described below, and the end product consists of predictions of enzyme behavior based on a structural model, which was verified by biochemical experimentation. The computer was a Silicon GraphicsO_2 work station, and the primary software package was Insight II (Accelerys, San Diego, CA) with the Homology, MODELER, Discover, Biopolymer, and SeqFold expansion modules. The first several modules are necessary for any type of homology or protein work. The SeqFold module is a sequence homology search engine that uses a threading technique to identify potentially homologous proteins based on predicted secondary structure of the target sequence and known secondary structures within structurally solved protein databases (*8*). All searches were performed against a nonredundant version of the Brookhaven PDB.

To create a protein model, SeqFold identified a homologue and then used the structure of that sequence homologue to map the sequence of the unknown structure to a set of 3D coordinates. This was done first on protein regions near the core and on well-conserved sections. The regions of poor conservation were then built onto the core using a fragment database and conformation searching techniques. The initial model was then optimized using a simulated annealing technique.

Evaluation of Protein Models. With the Insight II software package, homology-based models of primarily UGT1A10 and 1A7 were built. After running simulated annealing algorithms to optimize these protein models, feasibility of structure was evaluated, and images of these feasibility models were taken (not shown). The thickness of the backbone ribbon established PDB violation, which was a composite of chemical errors that included bond length, bond angle, steric overlap, and electrostatic potential such that a thicker ribbon indicated poorer conformation. Each image of the model showed optimization at three different times defined by a different color. The color of each ribbon related to the $\varphi-\psi$ angle violation of the amino acid backbone evident by bright colors that indicated disallowed conformation. Areas where the backbone was seen to diverge three ways were interpreted as areas of unstable conformation. Based on the data, visual evaluation of the protein backbone was possible. A predicted structure of the UDP-glcA binding site was ultimately derived from the models of UGT1A10 and 1A7 proteins (not shown). Whereas our model was suitable, we have evaluated it using a combination of mutational and Scatchard analyses of binding data of the radiolabeled affinity probe to partially purified 1A10-His and UGT1A7-His, as well as digestion and resolution of isozyme bound with labeled probe in a discontinuous SDS−polyacrylamide gel electrophoresis system.

Chemicals and Gels. Reagents for various analyses were of the highest available quality, including the Ni^{2+} affinity gel columns (Sigma).

Mutagenesis of UGT1A10 cDNA. To establish whether the predicted sites bound UDP-glcA, each residue was altered by site-directed mutagenesis (*4, 9*) of the full-length UGT1A10-cDNA as described in the Supporting Information using primers provided in Table 1S. All cDNA constructs were expressed in COS-1 cells, and cellular homogenates were tested for effects on activity.

The Glucuronidation Assay. Either the cellular homogenate of UGT1A10-His expressed in COS-1 or the partially purified protein was used in glucuronidation assays as previously described (*9*). Common donor substrate, UDP-[^{14}C]glcA (1.4 mM, 1.4 μCi/μmol), was used in all reactions with unlabeled acceptor substrate, mycophenolic acid (800 μM). Incubations contained 150 μg of protein at pH 6.4 or 7.6 for 2 h at 37 °C, and glucuronides were separated by thin layer chromatography as described (*9*). Product was quantified as previously described (*9*) using appropriate controls. Protein content was estimated using the BCA kit (Pierce, Rockford, IL), and product represents picomoles of glucuronide per milligram of protein per unit time.

Western Blot Analysis. To normalize for differences in expression of UGT1A10 and its mutants, antibody against the common end of the family A isozymes was used with Western blots that contained the proteins as described (*5*).

Inhibition of UGT1A10 by UDP-glc and UDP-hexanolamine. Kinetic analysis of inhibition of partially purified UGT1A10-His was carried out with UDP-glc and UDP-hexanolamine (Sigma, St. Louis, MO), which are both analogues of UDP-glcA (*10–12*). Increasing concentrations of UDP-glc or UDP-hexanolamine were added to the reaction mixture and allowed to stand for 10 min on ice before [^{14}C]UDP-glcA was added to start the reaction. Kinetic analysis was determined from the Lineweaver−Burk plot using Graph Pad Prism software (version 4).

Purification of UGT1A10His. After UGT1A10-transfected COS-1 cells expressed protein for 72 h, cells were harvested in PBS containing a cocktail of protease/phosphatase inhibitors (Sigma) and centrifuged. These inhibitors remained throughout the purification process. Packed cells were resuspended in 100 mM $KHPO_4$, pH 7.6, containing 6 mM CHAPS and 40 mM MDM, to solubilize the endoplasmic reticulum. Following centrifugation at 14000*g* for 10 min, the supernatant was centrifuged at 60000*g* for 30 min; the resulting supernatant containing 1A10-His was adjusted to pH 7.8 and applied to a His-select Ni^{2+} affinity gel (capacity 750 μg of protein/60 μL of packed resin in microspin columns), which had been preequilibrated in 0.1 M $KHPO_4$ (pH 7.6) with 0.01 M imidazole, 0.3 M NaCl, 6 mM CHAPS, 40 mM MDM, 100 μM sodium orthovanadate, and 5 mM sodium fluoride according to Sigma's protocol. After application of sample, the column was washed with 0.05 M $KHPO_4$ (pH 7.6) buffer containing 0.01 M imidazole, 0.3 M NaCl, and 6 mM CHAPS until OD_{280} reached background. UGT1A10 was eluted with 0.1 M $KHPO_4$ (pH 7.6) containing 0.3 M imidazole, 0.3 M NaCl, and 40 mM MDM. Eluted UGT1A10-His was dialyzed in a 10 kDa cutoff slide-A-lyzer

dialysis cassette (Pierce) against appropriate buffers (containing inhibitors described above) for 1 h before using in the UGT and $5N_3[\beta\text{-}^{32}P]$UDP-glcA binding assays. Our analysis indicated that UGT1A10 had been 200-fold purified relative to the 60000*g* supernatant protein.

Photoaffinity Labeling of UGT1A10-His Isozymes with $5N_3[\beta\text{-}^{32}P]$UDP-glcA. To determine binding of $5N_3[\beta\text{-}^{32}P]$UDP-glcA (Affinity Labeling Technologies, Lexington, KY) to UGT1A10-His, 15 μg aliquots of partially purified UGT1A10-His or 1A7-His in 0.1 M $KHPO_4$ (pH 7.6) buffer were incubated with increasing concentrations of $5N_3[\beta\text{-}^{32}P]$UDP-glcA (specific activity 0.2 Ci/mmol) that ranged between 0.2 and 2.0 mM in 50 μL reaction volume ((*13*). The mixture was UV irradiated with 254 nm light with a hand-held UV illuminator (model UVG-11; UVP Corp.) from a distance of 3 cm for 2 min; the irradiation was repeated after 5 min. Nonspecific binding was determined by exposure of 15 μg of isozyme to 0.5 or 2.0 mM nonlabeled $5N_3$UDP-glcA before irradiating for 2 min followed by exposure to 12.5 or 50 μM $5N_3[\beta\text{-}^{32}P]$UDP-glcA, respectively, before UV irradiation for 2 min. Duplicate reactions incubated at 4 °C for 15 min before filtering through phosphocellulose P81 membranes (Upstate) and washing with 5 mL of 0.75% phosphoric acid. Protein content was estimated using the BCA kit (Pierce, Rockford, IL).

Binding of the radiolabeled affinity ligand to UGT1A10-His and 1A7-His was carried out with 15 μg of purified isozyme with increasing concentrations from 30 μM to 10 mM $5N_3[\beta\text{-}^{32}P]$UDP-glcA as described above; protein was precipitated with 10% trichloroacetic acid, washed three times (1.2 mL) with 70% ethanol, air-dried, solubilized in Hydrofluor scintillation fluid (National Diagnostics), and counted.

Resolution of Peptides following Chemical Digestion of UGT1A10-His with Bound $5N_3[\beta\text{-}^{32}P]$UDP-glcA. Either partially purified UGT1A10-His or UGT1A7-His was exposed to $5N_3[\beta\text{-}^{32}P]$UDP-glcA as described above, pretreated with 1.0 mM dithiothreitol, and digested with NTCB (Sigma) in 4.0 M guanidine hydrochloride (*9*) for 72 h at 37 °C. (Based on UGT1A10 cysteine residues, NTCB digestion generated 15 fragments, ranging from 0.1 to 14.3 kDa.) Protein digest, concentrated by filtering through a G25 Sephadex column (Amersham-Bioscience), was solubilized in sample buffer (4% SDS, 12% glycerol, 50 mM Tris, 2% β-mercaptoethanol, and 0.01% Serva Blue G at pH 6.8) and resolved in a Tricine−SDS−polyacrylamide gel electrophoresis system (*14, 15*) concurrent with two sets of molecular mass markers that ranged between 1060 and 26000 Da and between 14 and 200 kDa. To detect radioactive ligand, gels were sliced in 1 mm sections and counted according to Cherenkov in a liquid scintillation counter. Data were processed and graphed with GraphPad prism software with background corrected.

RESULTS AND DISCUSSION

Previous attempts to find structurally determined proteins homologous to UGT isozymes to establish critical structures have essentially been unsuccessful. Although homologous proteins are present in the database, very few are membrane-bound, and only recently the *carboxyl*-terminal domain of ER-bound UGT predicted to interact with the common

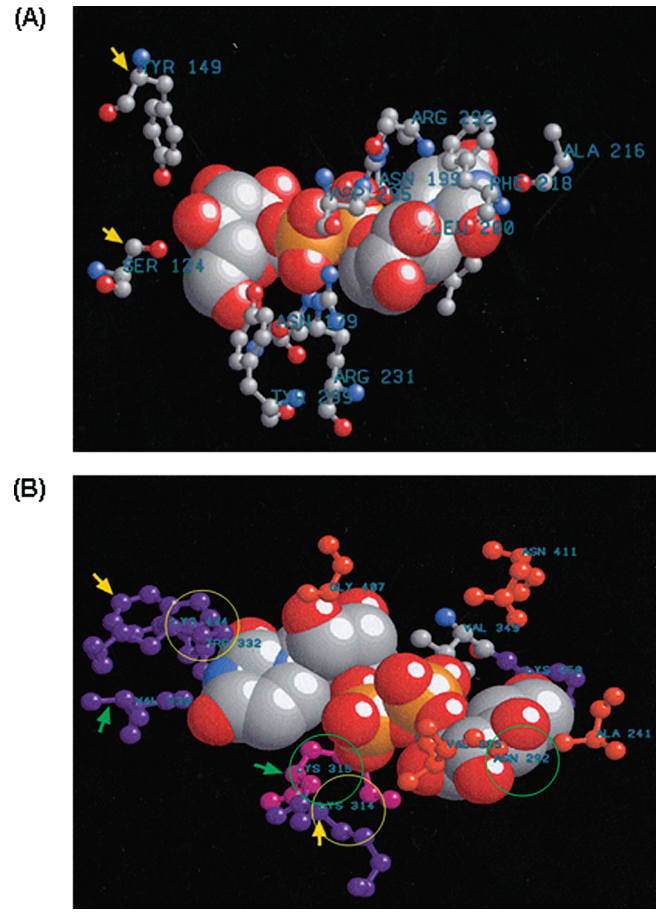

FIGURE 1: (A) Active site of 1XEL with the space-filling substrate, UDP-glc (*6*). (B) Image of UGT1A10 overlay on 1XEL with the bound space-filling form of UDP-glc. Arrows show the predicted active site amino acids with their positions. The model in the overlay of the unidentified domain of UGT1A10 predicts the binding residues circled as follows: left yellow circle, K404; lower yellow circle, K314; left green circle, K315; right green circle, N292.

substrate UDP-glcA was crystallized (*16*). As SeqFold is proficient at identifying structural homologues low on direct sequence−sequence identity to the target protein, it uncovered many low-identity homologues that bind similar substrates to UGT. Importantly, SeqFold discovered *E. coli* UDP-galactose 4-epimerase, designated PDB ID 1XEL (Supporting Information Figure 1S) to be the most prominent with the most chemically proper structure (Figure 1A) (*7*), which generated the best homology-based model of UGT1A10. The most highly homologous region of 1XEL and UGT1A10 is shown; that region of 1XEL is captured with a space-filling model of UDP-glc in association with its binding residues (S124, Y149, N179, N199, R231, and Y299) (Figure 1A) (*6*), which is clearly analogous to the UGT1A10 substrate, UDP-glcA. The image of UGT1A10 in an overlay onto 1XEL reveals, at least, part of the active site of 1A10 with the space-filling model of UDP-glc (Figure 1B). Primarily, the conserved Asn and three Lys residues, N292, K314, K315, and K404, appear critical in identifying the uracil diphosphoryl group in UDP-glc. K404 was shown to be proximal to K314 and K315 in the predicted UDP-glc binding pocket (Figure 1B). Alignment of residues in 1XEL and UGT1A10 is shown in Supporting Information Figure 1S. The residues colored purple in 1A10 are well conserved from 1XEL; residues in red are either not conserved or poorly

Table 1: K_i Values of UGT1A10 in the Presence of Inhibitors

inhibitor (concn)	K_m (mM)	K_i (mM)
no inhibitor	240	
UDP-glucose (10 mM)		2.2
UDP-hexanolamine (10 mM)		1.7

conserved, and the one in pink is a probable conservation that is uncertain due to an alignment gap (Supporting Information Figure 1S). In both cases the large molecule depicted in space-filling form in the center is the substrate molecule, UDP-glc, for 1XEL. In addition, an homology model of the *E. coli* dTDP glucose-4,6-dehydratase active site has been generated by combining its amino acid sequence alignment with the three-dimensional structure of 1XEL (*17*).

Effect of UDP-Containing Molecules on UGT1A10. Before carrying out studies with the affinity ligand, $5N_3$UDP-glcA, we determined the effect of two UDP-glcA analogues on 1A10. Initially, we show the K_m value (UDP-glcA) for 1A10 is 0.24 mM (Table 1). The Lineweaver−Burk plot shows both UDP-glc and UDP-hexanolamine caused competitive inhibition of 1A10 with K_i values of 2.2 and 1.7 mM, respectively (Figure 2, Table 1). [UDP-hexanolamine has been used as an affinity ligand for purifying UDP-glucuronosyltransferases in many studies (*10–12*).] Hence, the results with the two UDP-containing moieties gave a similar trend, indicating the sites are UDP-specific.

Effect of Mutations at Predicted UDP Binding Sites in UGT1A10-His. We examined the effect(s) of amino acid substitutions at predicted UDP-glcA binding site(s) in UGT1A10-His. All K314 mutants, K314E, K314A, K314R, K314Q, and K314G, caused null activity (Figure 3) using a radiolabeled-based assay that detected 50 pmol of product. By contrast, mutants at position 315 retained activity; conservative substitution K315R increased activity 40%, and nonconservative substitutions K315E, K315A, and K315G reduced activity up to more than 50% (Figure 3). The pattern of activity for K404 mutants was similar to that for K315 in that K404R and K404Q caused between 2.7- and 1.3-fold

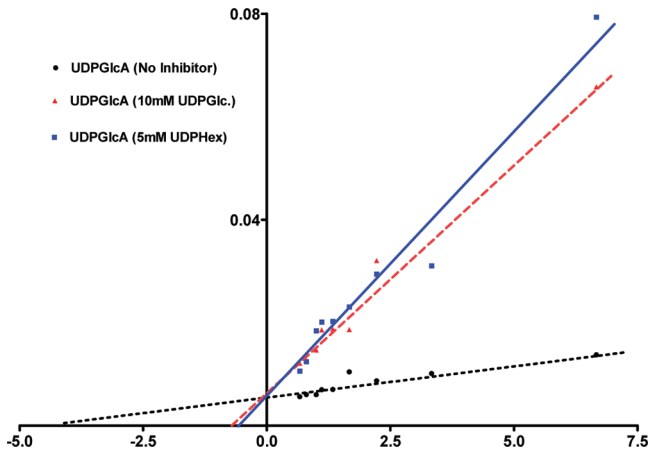

FIGURE 2: Lineweaver−Burk plot of UGT1A10 glucuronidation of mycophenolic acid. Glucuronidation of mycophenolic acid was carried out in the presence of increasing concentrations of UDP-glcA without or with 10 mM UDP-glc or 10 mM UDP-hexanolamine; product analysis was carried out as described under Materials and Methods. Activity is expressed as pmol/mg of protein/h. Experiments were repeated three times with standard errors between ±1% and 5%.

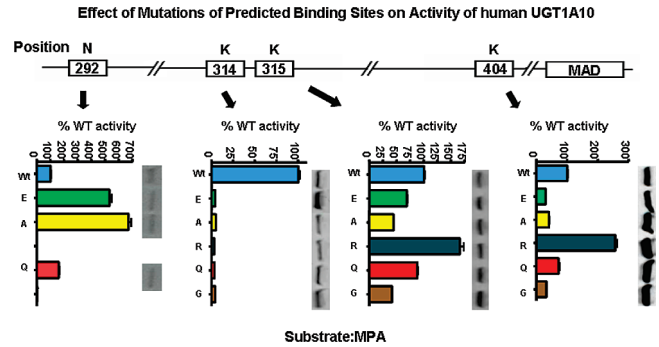

FIGURE 3: Effect of site-directed mutagenesis of predicted binding residues for UDP-glcA in UGT1A10. Based on the homology modeling in Figure 1B that identified potential UDP-glcA binding residues, N292, K314, K315, and K404 were altered by site-directed mutagenesis, and activity was determined as described under Materials and Methods. Activity for N292, K314, K315, and K404 is shown in color from left to right using mycophenolic acid as acceptor substrate. Activity was expressed as pmol/mg of protein/h; mutants were compared to wild type that represented 100%. Western blot analysis was carried out previously described (*4*). Experiments were carried out three times; standard errors are between ±1% and 5% as shown.

increase in activity, while the nonconservative substitutions K404E, K404A, and K404G caused between 68% and 75% loss of activity (Figure 3). Kinetic analysis demonstrated that 1A10 wild type and 1A10-K404R have nearly identical $K_{m(UDP\text{-}glcA)}$ values (data not shown). Null activity for all K314 mutants indicates that residue is critical to catalysis. Additionally, the greater reduction in activity for nonconservative substitutions, E, A, and G, at K315 and K404 compared to greater or no change in activity for conservative substitution, R and Q, at the same two positions provide strong evidence that a strong basic residue at both positions is important for UGT activity.

Conservation of Predicted UDP-glcA Binding Residues in UGTs. Because activity for K314 mutants was null and that for the K315R and K404R mutants increased 1.3−2.7-fold, respectively, we examined other UGT isozymes for conservation at these residues. In human, monkey, rat, and mouse, the *UGT1A* loci encode KK at positions 314 and 315 as shown in Supporting Information Figure 2S; K or R is at the equivalent position of 314/315, which is 321/322 for 2B isozymes (2B4, 2B7, 2B15, and 2B17), except for S at position 321/322 in both 2B15 and 2B17 and I at 321/322 in the inactive UGT8 isozyme (P. Mackenzie, personal communication). Similarly, K or R is at the equivalent position of 404 (K404 or R404) for both categories of UGTs; finally, position 292 is conserved with N292 or Q292 (Figure 2S). Hence, comparisons of equivalent residues in the *UGT1A* and *UGT2B* families for human, rat, and mouse at K314, K315, K404, and N292 show all are conserved, excluding the three isozymes cited. Since S321 in 2B15 and 2B17 was an exception compared to the 67 other UGTs, we have pursued studies with UGT2B15 and 2B17, which show the enzymes have suboptimal activity (R. Banerjee, J. Park et al. manuscript in preparation), a result that is consistent with our demonstration that the residue(s) is (are) at the UDP-glcA binding site and, thus, play(s) critical role(s) in the glucuronidation process.

Photoaffinity Labeling of Predicted $5N_3$[β-^{32}P]UDP-glcA Binding Sites in UGT1A10-His and UGT1A7-His. Since our results with mutants at the predicted binding sites affected

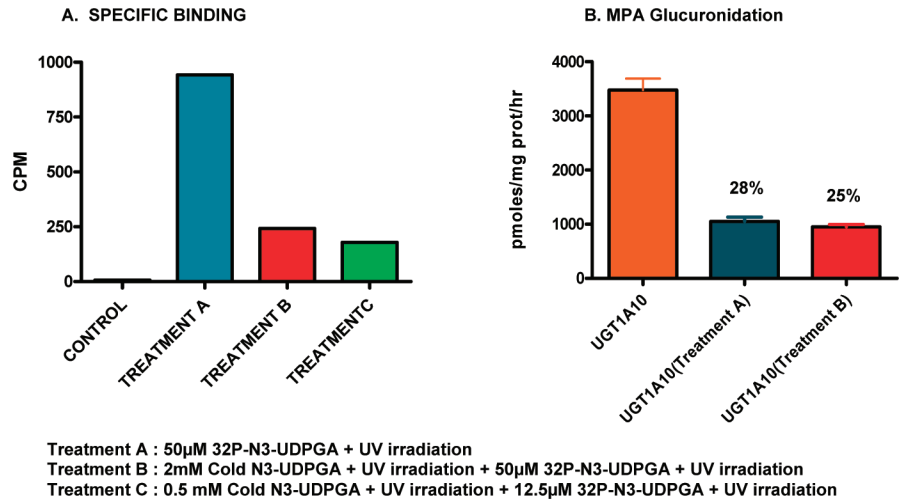

FIGURE 4: Specificity of $5N_3[\beta\text{-}^{32}P]$UDP-glcA binding to UGT1A10His. Details of exposure to nonlabeled and labeled $5N_3$UDP-glcA are as defined below the graph. Glucuronidation of mycophenolic acid is described under Materials and Methods. Binding, expressed as cpm/mg of protein, and activity were measured as described under Materials and Methods. Binding studies and activity measurements were repeated three times; standard errors ranged between ±1% and 5% as shown.

catalysis, we carried out binding studies with partially purified UGT1A10-His and 1A7-His isozymes. Initially, we established the specificity of the binding as shown in Figure 4. Treatment with either 0.5 or 2.0 mM $5N_3$UDP-glcA before adding 12.5 or 50 μM $5N_3[\beta\text{-}^{32}P]$UDP-glcA, respectively, nearly completely prevented both labeling of 1A10-His (Figure 4A) and its glucuronidation of MPA (Figure 4B), which established the level of nonspecific binding at ~25%. Because the N_3 (azido) group in uridine of $5N_3$UDP-glcA becomes a highly reactive nitrene following photolysis by UV irradiation, the nominally inactive UDP-sugar is activated and becomes covalently linked to the target protein backbone at the UDP-glcA site causing inactivation of the isozyme (Figure 4B).

Based on a Scatchard plot of $5N_3[\beta\text{-}^{32}P]$UDP-glcA binding to 1A10-His, both high and low affinity binding sites with negative cooperativity (Figure 5A) (*18, 19*) are evident. The B_{max} for high-affinity binding sites for partially purified 1A10-His (Figure 5A) is 30.25 nmol/mg of protein; the dissociation constant, K_d, was determined to be 6.94 μM (Table 2). Similarly, $5N_3[\beta\text{-}^{32}P]$UDP-glcA binding to 1A7-His also showed high- and low-affinity binding sites with negative cooperativity (*18, 19*) (Figure 5B); B_{max} for high-affinity binding sites for partially purified 1A7-His (Figure 5B) is 62.5 nmol/mg of protein; the dissociation constant, K_d, was determined to be 16.62 μM (Table 2). The plot also reveals that the low-affinity sites for both isozymes are not approaching saturation at 10 mM ligand concentration, which is consistent with results in Figure 4A that shows 25% nonspecific binding. Finding high- and low-affinity binding sites for $5N_3[\beta\text{-}^{32}P]$UDP-glcA in 1A10-His and 1A7-His agrees with UDP-[^{14}C]glcA binding to partially purified swine liver UGT in an earlier study that used forced dialysis (*19, 20*).

Identification of Binding Sites for $5N_3[\beta\text{-}^{32}P]$UDP-glcA in UGT1A10 and 1A7. To identify $5N_3[\beta\text{-}^{32}P]$UDP-glcA binding sites in UGT1A10, NTCB-digested affinity-labeled isozyme was resolved by electrophoresis in a discontinuous SDS−polyacrylamide gel (*14, 15*), which was sliced and counted. The results revealed two major peaks of radiolabel in the 11.3 and 14.3 kDa peptide fragments, respectively

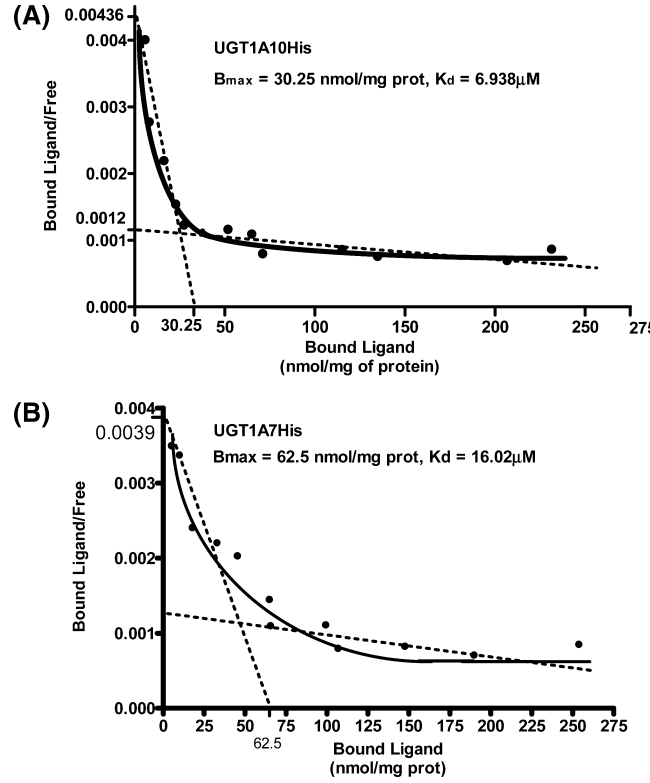

FIGURE 5: Binding the affinity ligand, $5N_3[\beta\text{-}^{32}P]$UDP-glcA, to partially purified (A) UGT1A10-His and (B) UGT1A7-His. The affinity ligand $5N_3[\beta\text{-}^{32}P]$UDP-glcA was added to 15 μg of partially purified isozyme and processed as described under Materials and Methods. Data were plotted according to Scatchard using GraphPad Prism software. B_{max} (high-affinity sites) and K_d values were calculated from the graph. Maximum binding for the high-affinity and low-affinity sites is defined by the intersections with the ordinate, and the calculated, K_d, is given in μM. Binding experiments were repeated four times.

(Figure 6A). Importantly, peptide molecular masses could be predicted on the basis of NTCB cleavage at reduced cysteine residues and defined in conjunction with molecular mass markers. Hence, it is predicted that the 11.3 and 14.3 kDa peptides contained K314/K315 and K404, respectively. Although samples were pretreated with dithiothreitol before NTCB digestion, we found small amounts of undigested 7.5

Table 2: Comparison of B_{max} and K_d of UGT1A10-His, 1A10K404R-His, and UGT1A7-His

	B_{max} (nmol/mg of protein)	K_d (μM)
UGT1A10-His	30.25	6.938
UGT1A10K404R-His	30.25	1.156
UGT1A7-His	62.50	16.02

kDa fragment (composed of the 4.2 and 3.3 kDa peptides) and an undigested 25.6 kDa fragment (composed of the 11.3 and 14.3 kDa peptides) (see Figure 6A,B). Similar analysis of the NTCB-digested affinity-labeled 1A10-K314A-His mutant showed both the 11.3 and 14.3 kDa peaks were abolished. Since R and E mutants at K404 showed 2.7-fold higher and 50% less activity, respectively, than wild type (Figure 3), we examined effects of $5N_3[\beta\text{-}^{32}P]$UDP-glcA binding to 1A10-K404R-His and -K404E-His by gel analysis. Compared to wild-type binding, Figure 6B shows that binding in the 14.3 kDa peptide is approximately 1.3-fold higher in 1A10-K404R-His and some 30% less for its K404E-His mutant, while the mutations had no apparent effect on the 11.3 kDa peptide (Figure 6B). Taken together, the facts that the null mutant, K314A, revealed loss of label in both the 11.3 and 14.3 kDa peptides and that label in the 14.3 kDa peptide for K404 mutants fluctuated in parallel with activity for -K404R-His and -K404E-His provided additional evidence that the critical K314 residue is in the 11.3 kDa peptide and that K404 is in the 14.3 kDa peptide in the discontinuous SDS−polyacrylamide gel electrophoresis system. Moreover, the results suggest the level of binding at K404 controls overall activity of the isozyme. Confirming the importance of K404 in UGT1A10, all UGTs contain either an R or K residue (Supporting Information Figure 2S), which is in agreement with our evidence that K404 in 1A10-His is a $5N_3[\beta\text{-}^{32}P]$UDP-glcA binding site.

Scatchard Analysis of $5N_3[\beta\text{-}^{32}P]$UDP-glcA Binding to UGT1A10-K404R-His and -K404E-His. Since mutational analysis in conjunction with binding data indicates K314 and K404 are located in the 11.3 and 14.3 kDa peptide, respectively, we compared 1A10-K404R-His and 1A10-K404E-His mutants bound with $5N_3[\beta\text{-}^{32}P]$UDP-glcA by Scatchard analysis to define better the effects at the two sites. Results show the K_d for the K404R mutant was reduced 6-fold (Table 2) accounting for the 2.7-fold increase in enzyme product (Figure 3), and B_{max} high-affinity binding sites were not affected; by contrast, K_d for K404E was not measureable (see Figure 6D), and its B_{max} decreased substantially (Figure 6D), accounting for the reduced activity.

Our results show that homology-based modeling by the Insight II SeqFold module identified a domain in *E. coli* UDP-galactose 4-epimerase (1XEL), which is structurally similar to a domain in 1A10. The image of the epimerase active site with the space-filling UDP-glc molecule (Figure 1A) and the overlay of 1A10 on 1XEL with its substrate, UDP-glc, identified the residues predicted to bind UDP-glcA in the human 1A10 isozyme. Moreover, the model is consistent with a domain in 1A10 that binds UDP-glcA based on predicted structural similarities. As shown in Supporting Information Figure 1S and Figure 1, computer analysis determined that residues S124, Y149, N179, N199, R231, and Y299 at the epimerase active site (*6*) are analogous to N292, K314, K315, and K404 in UGT1A10, which we confirmed biochemically. Evidence from (a) Scatchard analysis of UGT1A10-His and its mutants bound with the affinity ligand $5N_3[\beta\text{-}^{32}P]$UDP-glcA, (b) the null activity for K314 mutants, and (c) the parallel effects on activities and binding for UGT1A10-K404R and -K404E mutants, respectively, is an indication we have determined two critical residues involved in common donor substrate binding in UGT1A10. Because substitutions at N292 showed minimal effects on activity, evidence is not yet sufficient to indicate whether it plays a role in binding. The participation of strong basic residues, R231 and R292 (*6*; see Figure 4), at the active site of the epimerase via hydrogen bonding with the β-phosphoryl group in UDP-glc ((*6*), which is often seen with sugar transfers donated by UDP-sugar (*21–23*), is necessarily similar to UGT transfer of glucuronic acid flanking the β-phosphoryl group in UDP-glcA (*24*). It is suggested (*23*) that hydrogen bonding between the pyrophosphate in UDP-glc and an Arg and Ser at the active site serves to stabilize binding of the sugar donor in a transfer reaction. By analogy, it is possible that Arg/Lys serves a similar role in the transfer of glucuronic acid from UDP-glucuronic acid. In the case of the UDP-galactose 4-epimerase there is no sugar transfer. Instead, a hydride is abstracted from bound UDP-glc that reduces the NAD^+ cofactor resulting in a ketopyranose intermediate, which rotates in the active site, and the hydride is reintroduced into the opposite face of the ketopyranose intermediate generating an epimer of the sugar via a S_N reaction (*6*). Hence, the computer modeling is based on recognition and binding of the UDP moiety. In theory, it is possible that one or more predicted Lys residues are involved in UDP-glcA hydrogen bonding to facilitate cleavage/transfer of the glucuronic acid moiety.

Finally, null activity for all K314 mutants, which was consistent with loss of binding at both the 11.3 and 14.3 kDa peptide (Figures 3 and 6A), combined with parallel high and low activity for conservative and nonconservative substitutions, respectively, for K404 mutant (Figures 3) that affected only the 14.3 kDa peptide (Figure 6B), is strong evidence that both Lys residues are involved in catalysis but that K404 plays a less important role than K314 in activity/binding. Hence, our study has identified and confirmed that K314 and K404 play a critical role(s) in UGT1A10 binding and catalysis.

The observation that K/R314 or its equivalent position is strictly conserved in 67 out of 70 UGTs representing five species found at the UGT Web site (http://som.flinders.edu.au/FUSA/ClinPharm/UGT/) (Figure 2) is also compelling evidence that a strong base at that position is critical to UGT catalysis. Moreover, our comparisons show human *UGT2B15* and *UGT2B17* genes specify S321 (equivalent to K314 in 1A10) instead of K/R321 suggested these isozymes have suboptimal activity. Hence, detection of the active site via computer modeling in the absence of X-ray analysis of a crystalline structure of UGT identifies a critical amino acid substitution in both human UGTs that detoxify dihydrotestosterone. Further, a manuscript is under preparation that describes the suboptimal activity for UGT2B15 and 2B17 (*25*).

Evidence related to the level of activity versus basicity of residue 404 in various mutants and effects the same mutations have on affinity probe binding to UGT1A10-His and UGT1A7-His by Scatchard analysis indicate position 404

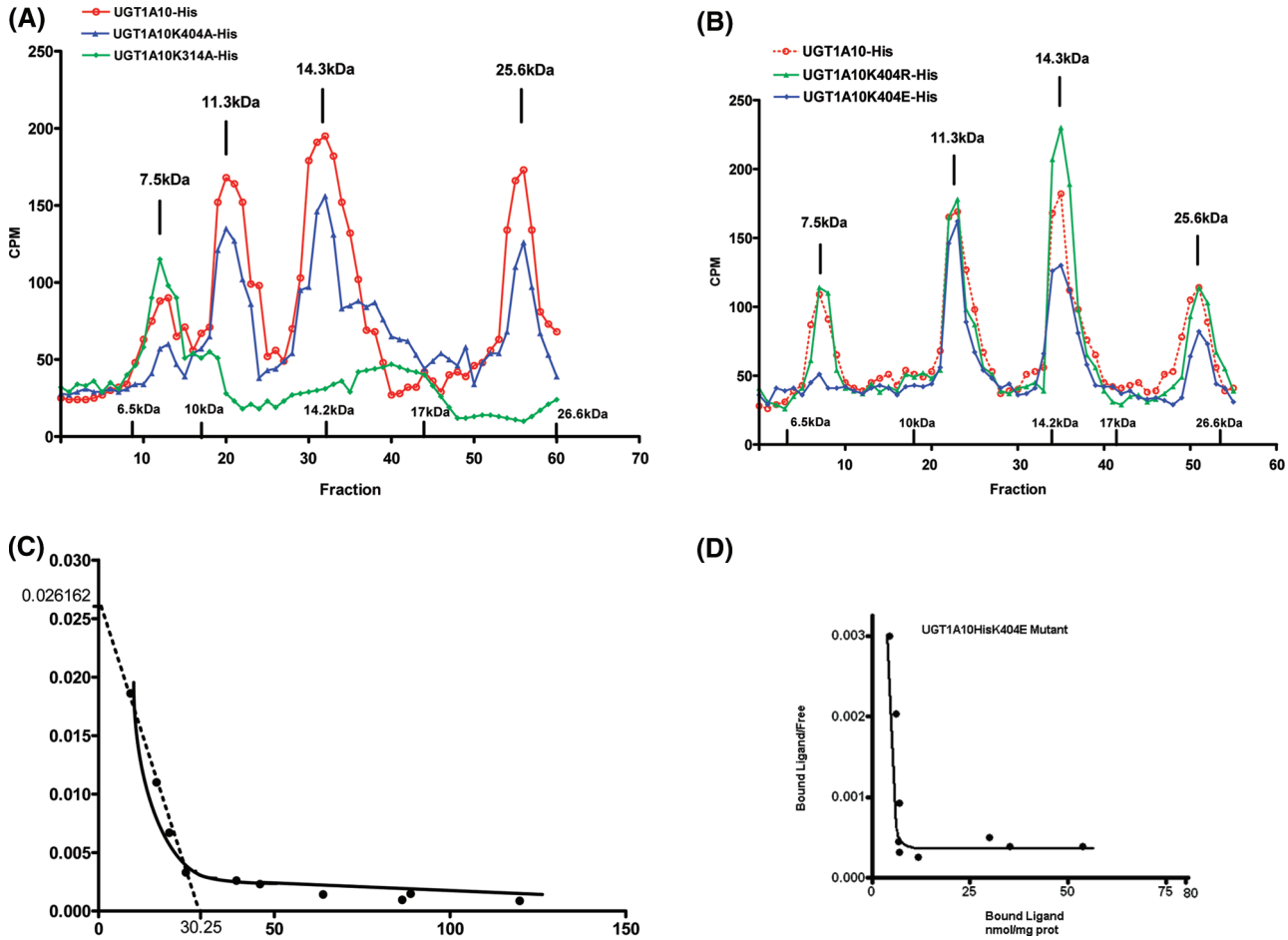

FIGURE 6: (A) Resolution of NTCB-digested UGT1A10-His, -K314A-His, and -K404A-His mutants bound with $5N_3[\beta\text{-}^{32}P]$UDP-glcA. The 11.3 and 14.3 kDa primary peptides contain K314 and K404 residues, respectively; 7.5 and 25.6 kDa peptides represent nondigestible 4.2 + 3.3 kDa and 11.3 + 14.3 kDa peptides, respectively. (B) UGT1A10-His, UGT1A10-K404R-His, and UGT1A10-K404E-His bound with $5N_3[\beta\text{-}^{32}P]$UDP-glcA. Each protein sample bound with the affinity ligand was NTCB-digested and resolved in a discontinuous SDS−polyacrylamide gel electrophoresis system as described under Materials and Methods with molecular mass markers as shown. Results represent bound cpm of $5N_3[\beta\text{-}^{32}P]$UDP-glcA in 1 mm gel fractions. (C) Scatchard analysis of UGT1A10-K404R-His or (D) UGT1A10-K404E-His binding to $5N_3[\beta\text{-}^{32}P]$UDP-glcA. Binding of the affinity ligand was processed and analyzed similar to samples described under Figure 5.

(Figure 6B) as a high-affinity site in UGT1A10 and 1A7. Finding the two peptides, 11.3 and 14.3 kDa, predictably contain K314 and K404, respectively, following resolution of NTCB-digested UGT1A10-His with bound $5N_3[\beta\text{-}^{32}P]$UDP-glcA in the discontinuous SDS−polyacrylamide gel system and their disappearance with similarly treated UGT1A10-K314A-His (Figure 6A) provide strong evidence that both K314 and K404 are high-affinity UDP-glcA binding sites. Evidence for high- and low-affinity UDP-glcA binding sites was detected previously using partially purified swine UGT (*19*).

A consideration of the study by Miley et al. (*16*) resulting from the crystallization of the bacterial-expressed carboxyl domain spanning residues 285 to 451 of human UGT2B7 identified many other residues when mutated in the intact protein that caused null or nearly null activity; this result suggests, therefore, that other residues are also associated with UDP-glcA binding. It is difficult to make meaningful comparisons of contact points for our space-filling UDP-glc in our homology-based UGT1A10 structure to those in the crystalline structure of UGT2B7 (*16*) carried out in the absence of UDP-glcA. Hence, residues other than strong bases, similar to those found at the active site of the UDP-galactose 4-epimerase (*6*), are possibly involved in UGT catalysis.

While this study confirmed, at least, two of the predicted four residues are involved in UDP-glcA interactions/binding in the UGT1A10 isozyme, mass spectrometric analysis studies are underway with purified UGT1A10 bound with the unlabeled affinity ligand to identify all residues involved in UDP-glcA binding.

ACKNOWLEDGMENT

We very much appreciate the assistance from Dr. Nikhil K. Basu for suggestions concerning site-directed mutagenesis.

SUPPORTING INFORMATION AVAILABLE

SeqFold alignment of UGT1A10 to 1XEL (Figure 1S), homologies of UGTs from different species focusing on regions surrounding amino acids 292, 314, 315, and 404 (Figure 2S), and primers for UGT1A10 Mutants (Table 1S). This material is available free of charge via the Internet at http://pubs.acs.org.

REFERENCES

1. Dutton, G. J. (1980) in *Glucuronidation of Drugs and Other Compounds* (Dutton, G. J., Ed.) pp 3−78, CRC Press, Boca Raton, FL.
2. Basu, N. K., Ciotti, M., Hwang, M. S., Kole, L., Mitra, P. S., Cho, J. W., and Owens, I. S. (2004) Differential and special properties of the major human UGT1-encoded gastrointestinal UDP-glucuronosyltransferases enhance potential to control chemical uptake. *J. Biol. Chem. 279*, 1429–1441.
3. Chen, F., Zhou, J., Ritter, J. K., Bondy, C. A., and Owens, I. S. (1996) Lobular distribution of human liver phenol and bilirubin uridine 5′-diphosphate glucuronosyltransferase messenger RNAs. *Gastroenterology 111*, 472–480.
4. Basu, N. K., Kole, L., and Owens, I. S. (2003) Evidence for phosphorylation requirement for human bilirubin UDP-glucuronosyltransferase (UGT1A1) activity. *Biochem. Biophys. Res. Commun. 303*, 98–104.
5. Basu, N. K., Kole, L., Basu, M., McDonagh, A. F., and Owens, I. S. (2007) Targeted inhibition of glucuronidation markedly improves drug efficacy in mice−A model. *Biochem. Biophys. Res. Commun. 360*, 7–13.
6. Thoden, T., Frey, P. A., and Holden, H. M. (1996) Molecular structure of the NADH/UDP-glucose abortive complex of UDP-galactose 4-epimerase from *Escherichia coli*: Implications for the catalytic mechanism. *Biochemistry 35*, 5137–5144.
7. Thoden, J. B., Hegeman, A. D., Wesenberg, G., Chapeau, M. C., Frey, P. A., and Holden, H. M. (1997) Structural analysis of UDP-sugar binding to UPD-galactose 4-epimerase from *Escherichia coli*. *Biochemistry 36*, 6294–6304.
8. Olsazewski, K. A., Yan, L., and Edwards, D. J. (1999) SeqFold−fully automated fold recognition and modeling software−evaluation and application. *Theor. Chem. Acc. 101*, 57–61.
9. Ciotti, M., and Owens, I. S. (1996) Evidence for overlapping active sites for 17α-e ethynlestradiol and bilirubin in the human major bilirubin UDP-glucuronosyltransferase. *Biochemistry 35*, 10119–10124.
10. Mackenzie, P. I., Hjelmeland, L. M., and Owens, I. S. (1984) Purification and immunochemical characterization of a low-pI form of UDP-glucuronosyltransferase from mouse liver. *Arch. Biochem. Biophys. 231*, 487–497.
11. Kanehara, H., Yokota, H., Sato, M., and Yuasa, A. (1992) Purification and properties of 4-hydroxybiphenyl UDP-glucuronosyltransferase from bovine liver microsomes. *J. Biochem. (Tokyo) 112*, 578–582.
12. Yokota, H., Yuasa, A., and Sato, R. (1988) Purification and properties of a form of UDP-glucuronosyltransferase from liver of 3-methylcholanthrene-treated rats. *J. Biochem. (Tokyo) 104*, 531–536.
13. Marazziti, D., Baroni, S., Fabbrini, L., Italiani, P., Catena, M., Dell'Osso, B., Betti, L., Giannaccini, G., Lucacchini, A., and Cassano, G. B. (2006) Binding of ^{3}H-Win-35,428 and ^{125}I-RTI-121 to human platelet membranes. *Neurochem. Res. 31*, 361–365.
14. Schägger, H., and von Jagow, G. (1987) Tricine-Sodium dodecyl sulfate-polyacrylamie gel electrophoresis for the separation of proteins in the range from 1 to 100 kDa. *Anal. Biochem. 166*, 368–379.
15. Hou, Z., Stapels., S. E., Haska, C., and Matherly, L. H. (2005) Localization of a substrate binding domain of the human reduced folate carrier to transmembrane domain 11 by radioaffinity labeling and cysteine-substituted accessibility methods. *J. Biol. Chem. 280*, 36206–36213.
16. Miley, M. J., Zielinska, A. K., Keenan, J. E., Bratton, S. M., Radominska-Pandya, A., and Redinbo, M. R. (2007) *J. Mol. Biol. 369*, 498–511.
17. Hegeman, A., Gross, J. W., and Frey, P. A. (2001) Probing catalysis by *Escherichia coli* dTDP-glucose-4,6-dehydratase: Identification and preliminary characterization of functional amino acid residues at the active site. *Biochemistry 40*, 6598–6610.
18. Price, N. C., and Stevens, L. (1999) in *Fundamentals of Enzymology: The Cell and Molecular Biology of Catalytic Proteins* (Price, N. C., and Stevens, L., Eds.) pp 235−237, Oxford Press, Great Britain.
19. Hochman, Y., Kelley, M., and Zakim, David. (1983) Modulation of the number of ligand binding sites of UDP-glucuronyltransferase by the gel to liquid-crystal phase transition of phosphatidylcholines. *J. Biol. Chem. 258*, 6509–6516.
20. Paulus, H. (1969) A rapid and sensitive method for measuring the binding of radioactive ligands to proteins. *Anal. Biochem. 32*, 91–100.
21. Horcajada, C., Guinovart, J. J., Fita, I., and Ferrer, J. C. (2006) Crystal structure of an archaeal glycogen synthase: Insight into oligomerization and substrate binding of eukaryotic glycogen synthases. *J. Biol. Chem. 281*, 2923–2931.
22. Ivanov, A. A., Fricks, I., Kendall Harden, T., and Jacobson, K. A. (2007) Molecular dynamics simulation of the P2Y14 receptor. Ligand docking and identification of a putative binding site of the distal hexose moiety. *Bioorg. Med. Chem. Lett. 17*, 761–766.
23. Thorse, K. S., Bak, S., Olsen, C. E., Imberty, A., Breton, C., and Mller, B. L. (2005) Determination of catalytic key amino acids and UDP-sugar donor specificity of the cyanohydrin glycosyltransferase UGT85B1 from sorghum bicolor. Molecular modeling substantiated by site-specific mutagenesis and biochemical analyses. *Plant Physiol. 139*, 664–673.
24. Fondueur-Gelinotte, M., Lattard, V., Oriol, F., Mollicone, R., Jacquinet, J.-C., and Mulliert, G. (2006) Phylogenetic and mutational analysis reveal key residues for UDP-glucuronic acid binding and activity of β1,3-glucuronosyltransferase I (GLCAt-I). *Protein Sci. 15*, 1667–1678.
25. Wright, F., Poizat, R., Bongini, M., Bozzalan, F., Doukani, and Mauvais-Jarvis, P. (1985) Decreased urinary 5 alpha-androstane-3 alpha, 17 beta-diol glucuronide excretion in patients with benign prostate hyperplasia. *J. Clin. Endocrinol. Metab. 60*, 294–298.

BI8006127